Coexistence of wrinkles and blisters in supported graphene

Kuan Zhang[1], Marino Arroyo*

LaCàN, Universitat Politècnica de Catalunya-BarcelonaTech (UPC), Barcelona 08034, Spain

Abstract

Blisters induced by gas trapped in the interstitial space between supported graphene and the substrate are commonly observed. These blisters are often quasi-spherical with a circular rim, but polygonal blisters are also common and coexist with wrinkles emanating from their vertices. Here, we show that these different blister morphologies can be understood mechanically in terms of free energy minimization of the supported graphene sheet for a given mass of trapped gas and for a given lateral strain. Using a nonlinear continuum model for supported graphene closely reproducing experimental images of blisters, we build a morphological diagram as a function of strain and trapped mass. We show that the transition from quasi-spherical to polygonal of blisters as compressive strain is increased is a process of stretching energy relaxation and focusing, as many other crumpling events in thin sheets. Furthermore, to characterize this transition, we theoretically examine the onset of nucleation of short wrinkles in the periphery of a quasi-spherical blister. Our results are experimentally testable and provide a framework to control complex out-of-plane motifs in supported graphene combining blisters and wrinkles for strain engineering of graphene.

Keywords: graphene, wrinkles, blisters, strain engineering

1. Introduction

Supported graphene exhibits out-of-plane deformations of different morphology and origin. Dislocations or grain boundaries in the graphene lattice can relax out-of-plane, creating a three-dimensional landscape in the nominally two-dimensional material [1, 2, 3]. Networks of localized wrinkles nucleate upon cooling of graphene grown by chemical vapor deposition (CVD) on metallic substrates [4, 5, 6, 7, 8]. Lateral strains can also be induced purposefully by a stretchable substrate, leading to individual wrinkles [9] or to massive crumpling of the supported graphene [10]. Here we focus on graphene blisters, created by gas molecules trapped between the substrate and the impermeable graphene surface. The trapped gas creates a significant pressure difference across the membrane that produces and stabilizes tense bubbles [11, 12, 13, 14, 15]. Because the deformation induced by wrinkles and blisters can strongly influence the electronic structure of graphene [16, 17, 14], they are often perceived as defects in an otherwise pristine graphene sheet [7, 9, 18]. It has been suggested, however, that these out-of-plane features could offer new functionalities by locally tuning the electronic, chemical, or optical properties of graphene by strain if they could be precisely controlled [17, 19, 20, 21, 14, 22].

Graphene blisters have been observed with different sizes and shapes. The reported radii of the circular edges of quasi-spherical blisters range from dozens of nanometers to several microns [11, 13]. By modifying the amount of gas released from the substrate into the interstitial space below the graphene membrane, the size quasi-spherical blisters has been controlled [13, 23]. In addition to quasi-spherical blisters with circular edges, polygonal blisters with straight edges have been observed, often in association with visible wrinkles emanating from its vertices [24, 25, 15]. Triangular and quadrangular straight-edged blisters have been observed and controlled by an external electric field[26]. Measurements of a very large pseudo-magnetic field generated by such a small triangular blister have demonstrated the ability of strain to engineer the electronic structure of graphene [27, 28, 17]. Figure 1(a-d) shows experimental observations of blisters of different morphology in supported graphene samples.

The mechanics of quasi-spherical blisters has been

*Corresponding author

Email address: Marino.Arroyo@upc.edu (Marino Arroyo)

[1]Current address: Department of Aerospace Engineering and Mechanics, The University of Minnesota, Minneapolis, MN 55455

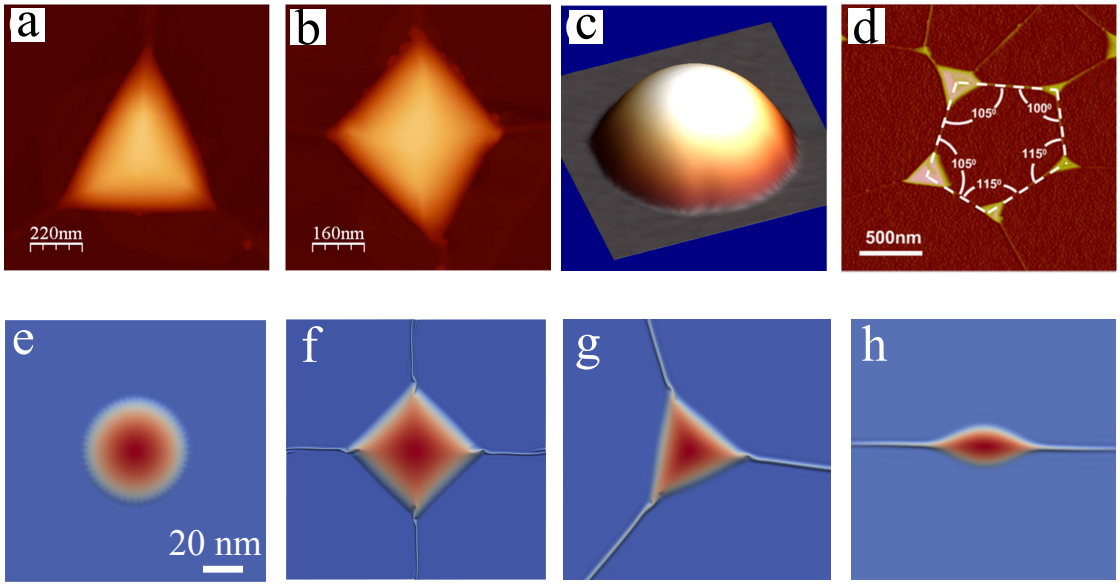

Figure 1: (a-c) Atomic Force Microscopy (AFM) topography scan of triangular, quadrangular and circular blisters [26]. In (a) and (b), wrinkles emanate from the vertices of the polygonal blisters. (d) A representative AFM image of straight-edged blisters coexisting with wrinkles.[24] (e-h) Various configurations of graphene blisters obtained from our simulations of supported graphene: circular (e), quadrangular (f), triangular (g) and lenticular (h) blisters. The colormap in (e-h) represents out-of-plane displacement.

previously examined in detail [29, 30, 31, 13]. However, the mechanisms leading to straight-edged blisters remains unexplored, despite numerous experimental observations. Furthermore, the coexistence and interaction between wrinkles and blisters has not been investigated. Here, we attempt to address these issues and provide a unified picture of blisters and wrinkles in supported graphene. Since lateral strain has been shown to produce networks of wrinkles and trapped gas has lead to controllable quasi-spherical blisters, we hypothesize that the morphology of the rim of blisters (either polygonal or circular) and their association with wrinkles result from the system trying to adopt energetically favorable configurations for a given compressive strain and number of interstitial molecules. To test this hypothesis and examine its consequences, we develop a computational model, described in Section II. In Section III, we build a morphological diagram depicting the coexistence of wrinkles and blisters. The mechanism of the morphological transition of blisters from quasi-spherical to straight-edged is examined in this section through simulations, and in Section IV through a theoretical model. The summary and outlook are given in Section V.

2. Modeling approach

We model the elasticity of graphene with an atomistic-based continuum theory combined with finite elements [32, 33], which has been shown to accurately and efficiently simulate graphene accounting for large deformations and buckling instabilities [34]. The interaction between graphene and substrate is modeled with a Lennard-Jones potential $\mathcal{V}(h)$ depending on the graphene-substrate separation h, with adhesion energy γ and equilibrium separation h_0 [35, 34]. Friction in the graphene-substrate interface is the fundamental mechanisms of load transfer between the substrate and graphene. Here, lateral strain is instead applied by the dimensions of our periodic domain. As we have previously discussed, friction can also have a significant influence on the spacing between wrinkles in laterally compressed supported graphene [22, 34]. However, for the configurations considered here, we have checked that the effect of friction is minor and thus ignore it in the present study. We include the effect of gas trapped between the graphene membrane and the substrate by modeling it as an ideal gas obeying the relation $pV = nRT$, where p is the pressure in the interstitial space, V the enclosed volume, n the number of gas molecules (in moles), R is the universal gas constant, and T the absolute temperature. In our simulations, we control the number of trapped gas molecules, i.e. nRT.

Temperature only enters the model through this relation; we ignore thermal fluctuations, which are small in supported or tense graphene membranes, but may influence the precise form of $\mathcal{V}(h)$ [36], and could slightly modify the stability of configurations studied later. Stable (in principle metastable) equilibrium states of the system are obtained by numerical minimization of the total potential energy of the system using a gradient-based quasi-Newton method. Details of the model and simulation methodology can be found elsewhere [22]. We consider a set-up consisting of a single and initially circular blister in equilibrium at the center of a 200×200 nm^2 periodic supported graphene sample. To prepare the system in this state, we artificially weaken the adhesion strength at the center of the sample and gradually increase nRT, in analogy with experiments [13]. Once the blister grows and delaminates from the substrate beyond the weakened region, we remove the adhesion defect and re-equilibrate the system. See Fig. 1(e) for a typical stable blister created with this procedure, which exhibits a circular rim.

Once a circular blister is created, by applying isotropic compressive strain (progressively reducing the lateral dimensions of the simulation cell), we observe quadrangular straight-edged blisters, associated with wrinkles emanating from its vertices, see Fig. 1(f). By adding trapped mass to a system with a pre-existing network of wrinkles, we computationally obtain triangular blisters with wrinkles emanating from the vertices, see Fig. 1(g). In the triangular and quadrangular blisters reported in [26] Fig. 1(a-b), a careful examination also suggests the presence of wrinkles originating at the vertices. By applying anisotropic strain to a quasi-spherical blister such as that in Fig. 1(e), we observe in simulations lenticular blisters coexisting with two collinear wrinkles, see Fig. 1(h), which have been recently reported experimentally [15]. The symmetry of our setup favors quadrangular blisters and pairs of wrinkles meeting at a 90° angle as in Fig. 1(f). Despite this bias, our modeling approach seems to capture the salient features of blisters in supported graphene. By focusing on the behavior of a single blister we examine in fact a system with a specific density of blisters given by the lateral dimensions of the periodic box. We will return to this discussion at the end of the manuscript.

3. A morphological diagram for the coexistenc of blisters and wrinkles

Based on a systematic set of simulations, see Fig. 2(b), we organize our observations in a morphological diagram in the compressive strain-trapped mass (ε_l, nRT) space, see Fig. 2(a), where ε_l represents the *linear compressive strain* applied in each direction. To explore this diagram, we start from a circular blister (white region) and increase ε_l while keeping nRT constant. We observe that short wrinkles nucleate at the periphery of the blister and gradually elongate until they reach the periodic boundary while the circular blister transits to a quadrangular straight-edged blister, see Fig. 2(i-iii). At this point, recalling the periodicity of the box, the system adopts a wrinkle network configuration with blisters at wrinkle junctions (light grey region). From this state, we go downward in the diagram by decreasing nRT and observe that the blister shrinks and finally collapses into a junction connecting the intersecting wrinkles along two orthogonal directions (dark grey region), see Fig. 2(v). Moreover, we find that this morphological diagram is largely path-independent. For instance, Fig. 2(a) shows with continuous and dashed lines two different paths in (ε_l, nRT) space, which intersect at configurations (iii) and (vi). It can be seen that the equilibrium state depends on the strain and trapped mass, but not on history. As illustrated in the figure, the transitions between different morphologies in the diagram, e.g. from circular blister to straight-edged blister coexisting with wrinkles, are gradual. For clarity, we represent them however as sharp lines in Fig. 2(a), where the criterion to distinguish between the white and the light grey regions is the nucleation of small wrinkles and the disappearance of small ripples at the periphery of the blister.

In the circular blister region, increasing/decreasing nRT results in larger/smaller blisters, which below a size threshold, become unfavorable compared to the planar configuration (i-vii-viii). Similarly, when compressive strain is reduced in configuration (v), the wrinkle height becomes smaller and at one point, the system transits to the planar configuration.

Interestingly, once the system gets trapped in the planar state (black region), the morphological diagram is no longer path independent. Indeed, if starting from the planar state we either increase ε_l or nRT, the system stays planar beyond the black region because the planar configuration is metastable with a significant barrier in a broader region. To estimate the region of metastability, we perform a linear stability analysis of the system around the planar state. We first consider the uniformly flat solution for a graphene sheet subjected to ε_c and nRT. The pressure within the interstitial space can be computed from the ideal gas law as

$$p = \frac{nRT}{\bar{h}A_0(1-\varepsilon_l)^2}, \tag{1}$$

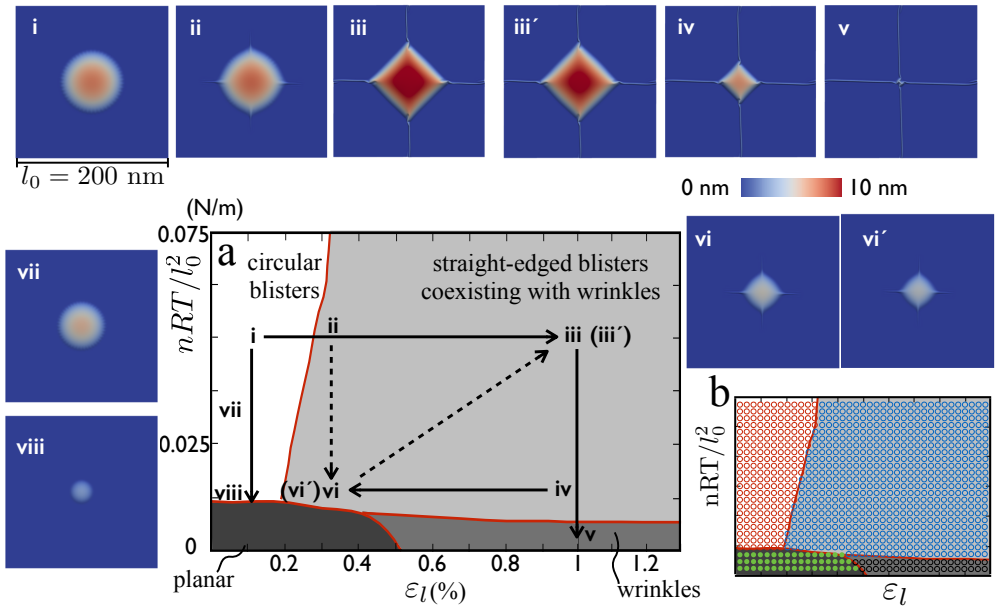

Figure 2: (a) Strain-trapped mass morphological diagram of a supported graphene periodic sample containing an initial quasi-spherical bubble. (i-iii) depicts the transition from a circular blister into a straight-edged blister coexisting with wrinkles, when the biaxially applied compressive strain is increased (ε_l represents the linear applied strain in each direction). Starting from (ii) and decreasing nRT, wrinkles shorten and the blister becomes small (vi). (iii' and vi') show the same blister configuration as (iii and vi), but accessed through an alternative path in parameter space. Starting from a straight-edged blister (iii) and decreasing nRT, the blister shrinks to become a junction connecting two intersected wrinkles (v). (vii and viii) depict shrinking circular blisters as nRT is decreased from (i). (b) Depiction of the points used to build the morphological diagram, where each state is equilibrated for fixed strain and trapped mass, and qualified according to its morphology.

where $\bar{h}$ is the equilibrium separation in the presence of pressure and A_0 is initial surface area of the unstrained graphene sheet. The pressure can also be computed from

$$p = \mathcal{V}'(\bar{h}). \tag{2}$$

Equating both expressions for p, we obtain an implicit formula for $\bar{h}$, which can be solved numerically given ε_l and nRT. We can then linearize the system around this equilibrium configuration and assess its stability. In the present situation, the linearized van der Waals potential takes the form

$$\hat{\mathcal{V}} = \frac{\gamma}{2h_0^2}\left[-18\left(\frac{h_0}{\bar{h}}\right)^5 + 45\left(\frac{h_0}{\bar{h}}\right)^{11}\right]w^2, \tag{3}$$

where h_0 is the equilibrium separation of the Lennard Jones potential in the absence of a pressure difference across the membrane, and w is the out-of-plane displacement. Equation (3) reflects the fact that this potential softens as nRT ($\bar{h}$) increases. This linear stability analysis provides a critical strain for the onset of instability of the planar state

$$\hat{\varepsilon}_{cr} = -\frac{2}{h_0\bar{Y}}\sqrt{\left[-18\left(\frac{h_0}{\bar{h}}\right)^5 + 45\left(\frac{h_0}{\bar{h}}\right)^{11}\right]\gamma D}, \tag{4}$$

where we introduce $\bar{Y} = Y_s/(1-\nu^2)$, $Y_s = 336\text{N m}^{-1}$ is the surface Young's modulus (with units of line tension), and $D = 0.238$ nN nm is the bending modulus. Equation (4) depends on nRT through $\bar{h}$.

This equation allows us to delimit the region of marginal stability of the planar configuration in the morphological diagram as a blue curve in Fig. 3. We test with fully nonlinear calculations this boundary for meta-stability of the planar state. Starting at the origin of the diagram, we increase both strain and trapped mass to describe a diagonal path. As predicted by the estimate, we find that the system abruptly transits from the planar state to a state where blisters coexist with wrinkles when the diagonal path intersects the blue stability boundary (ix). If instead we increase only strain, we find that in agreement with the morphological diagram the system transits to a wrinkled configuration as we reach the marginal stability threshold (x). To leave the metastable planar state, the system now needs to nucleate new out-of-plane features, rather than transform a pre-existing feature such as in Fig. 2. The precise morphology of states (ix) and (x) is very sensitive to computational details such as the size of the periodic box, the mesh or the numerical tolerance, but the general fea-

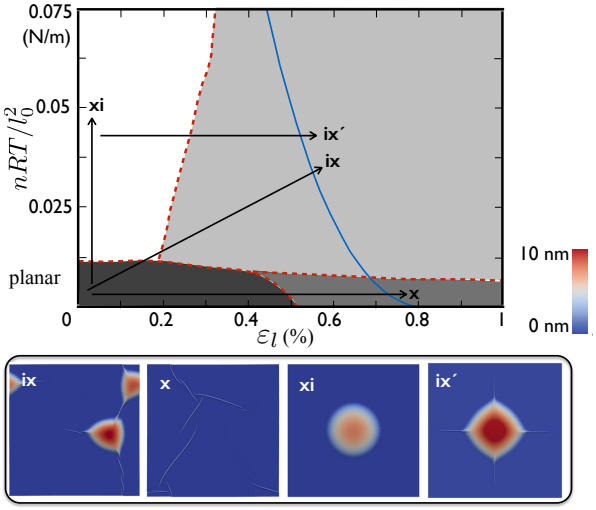

Figure 3: Starting from a planar state and increasing both nRT and ε_l, the graphene surface buckles into polygonal blisters that coexist with wrinkles (ix). With only compressive strain, a planar surface buckles into a network of localized wrinkles (x). By only increasing nRT, the nucleation of a circular blister (xi) requires small defect in the substrate. Starting from a point around (xi) and increasing ε_l, we obtain state (ix'), close to (ix) in terms of strain and enclosed gas mass. These two states exhibit significantly different morphology, exemplifying that, once the system visits the planar state, the proposed diagram is path-dependent.

tures of the solution, in terms of coexistence straight-edged blisters and wrinkles or energy contributions, is objectively captured by the computational model. See our discussion in a previous paper [22]. If we increase only trapped mass within the range of our plot, we cannot exit the region of marginal stability of the planar state and no blister formation is observed. However, a small defect, e.g. in the graphene-substrate adhesion, can facilitate the nucleation of a circular blister (xi). Starting from this blister, we increase strain until we arrive at a state (ix') nominally equivalent to (ix) in terms of strain and trapped gas mass. It can be observed, however, that this state is morphologically very different from (ix) very different morphology, showing in what sense the diagram is path-dependent when the system visits the planar state and needs to re-nucleate out-of-plane features.

We discussed in our previous paper [22] that wrinkle network formation could be interpreted as a process of stretching energy relaxation and focusing into small localized deformation features. To analyze whether analogous mechanisms are also operative here, we investigate next the energetics of the transition between a circular blister and a straight-edged blister coexisting with wrinkles, as shown in Fig. 2(i-iii). A quasi-spherical blister is doubly curved, and therefore the Gauss Egregium Theorem implies that such a configuration is necessarily stretched. Such stretching is energetically penalized by graphene's extreme in-plane stiffness. Figure 4(a) shows a map of the stretching energy density, which is significant and spreads over the entire blister and part of the adhered region in its vicinity. This figure also shows how the system partially relaxes the stretching energy at the periphery of the blister by slightly rippling. Figure 4(b) shows how, as strain is progressively increased, the transition towards a straight-edged blister with radial wrinkles relaxes the stretching energy in the blister, but focuses stretching energy in small regions where the blisters and wrinkles meet. When the blister us fully polygonal, Fig. 4(c), this mechanism is exacerbated with nearly zero stretching energy throughout the sample, except for a weakly stretched region at the top of the blister and tiny but highly stretched features at the wrinkle-blister connections. Figure 4(d) shows the variations of the different components of the energy (in-plane stretching, bending and adhesion) per unit area as a function of compressive strain. The sharp drop in stretching energy in this plot corresponds to the moment when the wrinkles extend to the boundary of the periodic domain. These results confirm the depiction of this process as one of stretching energy relaxation and focusing, at the expense of bending and adhesion energy.

A critical step in the transition from circular to straight-edged blisters is the nucleation of short wrinkles at the periphery of the blister. To shed light into the onset of this process, we analyze next in detail the stress state in this region for a circular blister.

4. Theoretical analysis of the transition from a circular to a polygonal blister

During this transition from circular to straight-edged blisters, thin and short wrinkles nucleate near the periphery of the blister. This buckling event is governed by the biaxial strain conditions near the periphery of the blister. To examine this process, we develop next an simple analytical model, related to previous models of supported graphene blisters [31, 13]. Clamped boundary condition of the blister edge are commonly assumed, and leading to zero hoop strain where these wrinkles form. However, a compressive hoop strain can develop due to the the sliding of the blister boundary [30]. The compressive hoop strain near the periphery of the blister can trigger the nucleation of wrinkles. Here, we consider this in-plane sliding of graphene near the blister edge, and include in the analysis the outer annular region of graphene adhered to the substrate. As

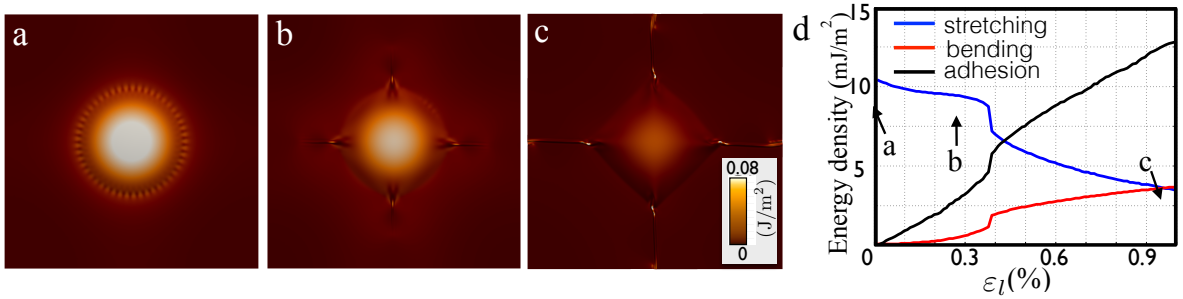

Figure 4: (a-c) In-plane stretching energy density during the transition from a circular blister into a straight-edged blister, shown earlier in Fig. 2 (i-iii). (d) A plot of different energy components when the applied compressive strain is increased.

commonly done [31], we approximate the out-of-plane profile of the blister as

$$z(r) = \delta\left(1 - \frac{r^2}{a^2}\right), \tag{5}$$

for an axisymmetric blister of radius a and maximum deflection δ, both to be determined. We assume a cubic distribution of radial displacement

$$u(r) = \left(u_0 + u_1\frac{r}{a}\right)\frac{r}{a}\left(1 - \frac{r}{a}\right) + u_p\frac{r}{a}, \tag{6}$$

where u_0 and u_1 are the parameters to be determined, and u_p accounts for the in-plane sliding of the blister edge. Equations (5) and (6) offer a reasonable approximation to the deformation of relatively large blisters. In the von Karman theory, accounting for the nonlinear effect of the out-of-plane displacement $z(r)$, the radial and hoop strains adopt the form [37]

$$\varepsilon_r(r) = \frac{\partial u}{\partial r}(r) + \frac{1}{2}\left[\frac{\partial z}{\partial r}(r)\right]^2, \tag{7}$$

$$\varepsilon_t(r) = \frac{u(r)}{r}. \tag{8}$$

Recalling Equations (5) and (6), the radial and hoop strain can be written as

$$\varepsilon_r(r) = \left(\frac{u_0}{a} + \frac{u_1 r}{a^2}\right)\left(1 - \frac{2r}{a}\right) + \frac{u_1 r}{a^2}\left(1 - \frac{r}{a}\right) + \frac{2\delta^2 r^2}{a^4} + \frac{u_p}{a}, \tag{9}$$

$$\varepsilon_t(r) = \left(\frac{u_0}{a} + \frac{u_1 r}{a^2}\right)\left(1 - \frac{r}{a}\right) + \frac{u_p}{a}. \tag{10}$$

Note that the hoop strain in Equation (10) is in general not zero at the periphery ($r = a$), as controlled by the sliding displacement u_p. We can now derive the elastic strain energy per unit area in the blister as

$$U_s^{in}(r) = \frac{\bar{Y}}{2}(\varepsilon_r^2 + 2\nu\varepsilon_r\varepsilon_t + \varepsilon_t^2). \tag{11}$$

In the current membrane model, we ignore the bending stiffness of the film. This approximation is computationally convenient and valid for relatively large blisters. The pressure of gas inside the blister has the following contribution of free energy density,

$$U_g(r) = -zp. \tag{12}$$

Next, we consider the annular region outside of the blister, which is adhered to the substrate, and has the inner radius a, and outer radius b. The radial and hoop components of stress follow the general form [37]

$$\begin{aligned}\sigma_r &= \frac{A}{r^2} + 2C,\\ \sigma_t &= -\frac{A}{r^2} + 2C,\end{aligned} \tag{13}$$

and the radial displacement in the region $a < r < b$ is

$$u = \frac{1}{Y_s}\left[-\frac{(1+\nu)A}{r} + 2C(1-\nu)r\right]. \tag{14}$$

In this region, we impose the Dirichlet boundary conditions $u(b) = \varepsilon_l b$ and $u(a) = u_p$, see Equation (6). Combining these boundary conditions with Equation (14), we obtain

$$A = \frac{Y_s}{1+\nu}\frac{ab^2}{b^2 - a^2}(u_p - a\varepsilon_l), \tag{15}$$

$$2C = \frac{Y_s}{1-\nu}\frac{b^2\varepsilon_l - au_p}{b^2 - a^2}. \tag{16}$$

Recalling Equation (13) and the expressions for A and C, we can compute stretching energy density of the annular region outside of the blister as

$$U_s^{out}(r) = \frac{1}{2Y_s}(\sigma_r^2 + \sigma_t^2) - \frac{\nu}{Y_s}\sigma_r\sigma_t. \tag{17}$$

Considering now the entire system consisting of the blister and the annular region, and including the effect

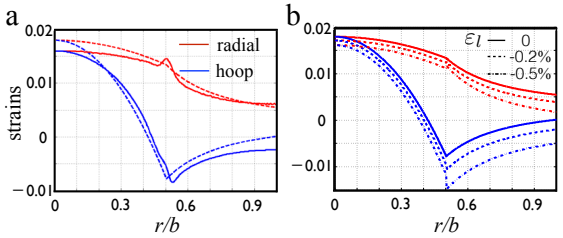

Figure 5: (a) Comparison between the theoretical model (dotted lines) and the nonlinear simulations (solid lines) for the radial and hoop components of the strain. (b) Distribution of the radial and hoop components of the strain when the applied strain ε_l is progressively increased. The hoop strain develops increasing compression near the periphery of the blister.

of the adhesion energy per unit surface γ, we obtain the total energy as

$$\Pi(a,\delta,u_0,u_1,u_p) = 2\pi\int_0^a \left(U_s^{in}+U_g\right)rdr + 2\pi\int_a^b \left(U_s^{out}+\gamma\right)rdr. \qquad (18)$$

By minimizing the total energy Equation (18) with respect of a,δ,u_0,u_1,u_p, stable equilibria are obtained. The distribution of the two components of strain is shown in Fig. 5(a), and compared with our fully nonlinear simulations. Despite the simplicity of the theoretical model, the fact that our periodic computational domain is square (as opposed to the disc-like geometry of the simple model), and the modest size of the blister (and therefore bending energy plays a role), the agreement between model and simulations is quite good. We see that at the periphery of the blister, the strain is negative (compressive) in hoop direction, and positive in radial direction. These negative hoop strains are consistent with the small ripples always present in our simulations in at the edge of the detached part of quasi-spherical blisters. The model also shows that the compressive hoop strain increases as ε_l increases. Such high compressive hoop strains could favor the nucleation of small wrinkles near the periphery of the blister, and trigger the morphological evolution from a circular blister to a straight-edged blister in Fig. 2(i-iii).

We analyze next the onset of instability at the rim of such a circular blister. For supported graphene under uniaxial compression, a linear instability analysis has been proposed in many previous studies, predicting a critical strain upon which the planar surface transforms to rippling. With further compression, the uniformly distributed rippling will transit to several localized wrinkles due to the nonlinearity of van der Waals interaction [34]. However, the periphery of the blister experiences

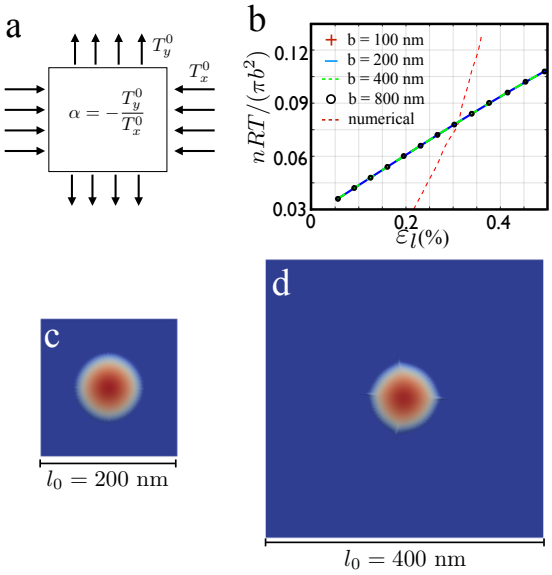

Figure 6: (a) Simplified model for the state of the graphene sheet at the periphery of the blister, under compression in the x direction (the azimuthal direction) and stretching in y (radial) direction. (b) Theoretical estimation of the boundary between the white (circular blister) and light grey (straight-edged blister with wrinkles) regions in the phase diagram in Fig. 2 with various sizes of the domain. The boundary between these two states as delimited in Fig. 2 is shown with a red-dashed line. Despite the differences between the two models (shape of domain, criterion for the transition, effect of curvature of the rim neglected in the model, etc.), the simple theoretical model captures the trends of the transition and explains the underlying mechanism. Panel (b) predicts that, under the same value of nRT = 2500 nN·nm and ε_l = 0.15%, for an array of blisters of high density (smaller domain size, c), the quasi-spherical blister is more stable than for a lower density of blisters (larger domain size, d). This prediction is tested computationally in (c) and (d).

a biaxial strain state, compressive along the azimuthal direction and tensile in the radial direction. We examine next the onset of buckling under such biaxial strain, ignoring the effect of the curvature of the blister edge.

Consider a supported rectangular graphene sheet compressed in one direction and stretched in the other direction Fig. 6(a). The stretching delays the critical strain of rippling without changing the rippling direction or wavelength. We denote by $u(x,y)$ and $v(x,y)$ the in-plane displacements and $w(x,y)$ the out-of-plane displacement of the membrane, and ε_x and ε_y the in-plane strain components in x and y directions. The stretching and bending energies of the membrane per unit area can be expressed as

$$U_s = \frac{\bar{Y}}{2}(\varepsilon_x^2+\varepsilon_y^2+2\nu\varepsilon_x\varepsilon_y),$$
$$U_b = \frac{D}{2}\left(\frac{\partial^2 w}{\partial x^2}\right)^2. \qquad (19)$$

Adopting a von Karman nonlinear plate theory [37], the membrane strain components of the film can be approximated as

$$\varepsilon_x = \varepsilon_x^0 + \frac{\partial u}{\partial x} + \frac{1}{2}\left(\frac{\partial w}{\partial x}\right)^2, \qquad \varepsilon_y = \varepsilon_y^0 + \frac{\partial v}{\partial y} + \frac{1}{2}\left(\frac{\partial w}{\partial y}\right)^2, \tag{20}$$

where ε_x^0 and ε_y^0 represent the globally applied lateral strain on the membrane. We assume uniaxial ripples perpendicular to the direction of compressive strain as $w(x) = A\cos(kx)$. By requiring the uniformity of the in-plane tension or strain, see Eq. (20), the in-plane displacement in x becomes $u(x) = (1/8)k^2A^2\sin(2kx)$, and the constant strain component in x becomes $\varepsilon_x = \varepsilon_x^0 + (1/4)k^2A^2$. In the y direction, $\varepsilon_y = \varepsilon_y^0$. The stretching energy difference per unit area takes the form

$$\begin{aligned}\Delta\bar{U}_s(A,k) =& \frac{\bar{Y}}{2}(\varepsilon_x^2 + \varepsilon_y^2 + 2\nu\varepsilon_x\varepsilon_y - \varepsilon_x^{0^2} - \varepsilon_y^{0^2} - 2\nu\varepsilon_x^0\varepsilon_y^0)\\ =& \frac{T_x^0}{4}k^2A^2 + \frac{\bar{Y}}{32}k^4A^4 + \frac{T_y^0}{4}\nu k^2A^2,\end{aligned} \tag{21}$$

where $T_x^0 = \bar{Y}\varepsilon_x^0$ and $T_y^0 = \bar{Y}\varepsilon_y^0$ are reference surface tensions in the x and y directions. The third term in Eq. (21) is the contribution in the stretching energy of the applied stretch in the y direction. Including the bending and adhesion energies, the total energy difference per unit area then becomes

$$\Delta\bar{U}(A,k) = \left(\frac{T_x^0 + T_y^0\nu}{4}k^2 + \frac{D}{4}k^4 + \frac{27\gamma}{4h_0^2}\right)A^2 + \frac{\bar{Y}}{32}k^4A^4. \tag{22}$$

If $T_y^0 = -\alpha T_x^0$, we have

$$\varepsilon_{cr} = -\frac{2}{h_0\bar{Y}(1-\alpha\nu)}\sqrt{27\gamma D}, \tag{23}$$

which predicts the critical strain along x.

The membrane theory developed earlier in the paper provides an estimate of the strain state at the periphery of the blister, i.e. ε_x and α, given the applied strain ε_l and nRT. Using the equation above to estimate the onset of buckling instability at the margin of a quasi-spherical blister, we can theoretically estimate the boundary between the white (circular blister) and light grey (straight-edged blister with wrinkles) regions in the phase diagram in Fig. 2. This theoretical estimate of the boundary is represented in Fig. 6(b). Despite all the approximations in the model and the somewhat arbitrary criterion to select the boundary in Fig. 2, we observe that the theoretical prediction for the transition captures the general trend observed in the numerical calculations. Interestingly, it can be observed that when plotting *nRT per unit area* versus ε_l, the boundary does not change as the size of the domain changes. Since the size of the domain can be interpreted as the separation between blisters in a graphene sample, we can conclude that the transition strain between circular and straight-edged blisters for a given number of trapped molecules per unit graphene area is independent of blister density. This observation allows us to estimate the transition from circular blisters to straight-edged blisters for very large domain sizes, beyond the limits of our computational capabilities. Furthermore, the relation represented in Fig. 6(b) predicts that for a given nRT and ε_l, circular blisters are more stable if the domain size is smaller. Figures 6(c) and 6(d) show an example of this behavior, where for the larger domain size, wrinkles have nucleated at the periphery of the blister.

5. Summary and outlook

We have examined the coexistence of wrinkles and blisters in supported graphene. We have shown that a wide diversity of out-of-plane disturbances observed in supported graphene, including spherical blisters, wrinkles, and polygonal blisters, can be explained within a unified framework accounting for the lateral strain and for the trapped mass beneath the graphene sample.

We have proposed a morphological diagram organizing the behavior of the system. The transition between quasi-spherical blisters to straight-edged blisters upon increasing compressive strain can be understood as a process of stretching energy relaxation and focusing. A simple theoretical model suggest that the onset of this transition is determined by compressive hoop strains at the periphery of the blister caused by radial sliding. This model predicts that the critical compressive strain to transition between circular and straight-edged blisters for a given number of trapped molecules per unit graphene area is independent of blister density. Our results provide a number of experimentally testable predictions and a framework to control complex out-of-plane motifs in supported graphene combining blisters and wrinkles.

Acknowledgments

We acknowledge the support of the European Research Council under the European Community's 7th

Framework Programme (FP7/2007-2013)/ERC grant agreement nr 240487. KZ acknowledges the support of the UPC. MA acknowledges the support received through the prize "ICREA Academia" for excellence in research, funded by the Generalitat de Catalunya.

References

[1] Y. Liu, B. I. Yakobson, Cones, pringles, and grain boundary landscapes in graphene topology, Nano Letters 10 (6) (2010) 2178–2183.

[2] B. I. Yakobson, F. Ding, Observational geology of graphene, at the nanoscale, ACS Nano 5 (3) (2011) 1569–1574.

[3] T. Zhang, X. Li, H. Gao, Defects controlled wrinkling and topological design in graphene, Journal of the Mechanics and Physics of Solids 67 (0) (2014) 2 – 13.

[4] X. Li, W. Cai, J. An, S. Kim, J. Nah, D. Yang, R. Piner, A. Velamakanni, I. Jung, E. Tutuc, S. K. Banerjee, L. Colombo, R. S. Ruoff, Large-area synthesis of high-quality and uniform graphene films on copper foils, Science 324 (5932) (2009) 1312–1314.

[5] A. W. Robertson, A. Bachmatiuk, Y. A. Wu, F. Schäffel, B. Büchner, M. H. Rümmeli, J. H. Warner, Structural distortions in few-layer graphene creases, ACS Nano 5 (12) (2011) 9984–9991.

[6] A. N. Obraztsov, E. A. Obraztsova, A. V. Tyurnina, A. A. Zolotukhin, Chemical vapor deposition of thin graphite films of nanometer thickness, Carbon 45 (2007) 2017–2021.

[7] W. Zhu, T. Low, V. Perebeinos, A. A. Bol, Y. Zhu, H. Yan, J. Tersoff, P. Avouris, Structure and electronic transport in graphene wrinkles, Nano Letters 12 (7) (2012) 3431–3436.

[8] M. Liu, Y. Zhang, Y. Chen, Y. Gao, T. Gao, D. Ma, Q. Ji, Y. Zhang, C. Li, Z. Liu, Thinning segregated graphene layers on high carbon solubility substrates of rhodium foils by tuning the quenching process, ACS Nano 6 (12) (2012) 10581–10589.

[9] T. Jiang, R. Huang, Y. Zhu, Interfacial sliding and buckling of monolayer graphene on a stretchable substrate, Advanced Functional Materials 24 (2013) 396–402.

[10] J. Zang, S. Ryu, N. Pugno, Q. Wang, Q. Tu, M. J. Buehler, X. Zhao, Multifunctionality and control of the crumpling and unfolding of large-area graphene, Nature Materials 12 (2013) 321–325.

[11] E. Stolyarova, D. Stolyarov, K. Bolotin, S. Ryu, L. Liu, K. T. Rim, M. Klima, M. Hybertsen, I. Pogorelsky, I. Pavlishin, K. Kusche, J. Hone, P. Kim, H. L. Stormer, V. Yakimenko, G. Flynn, Observation of graphene bubbles and effective mass transport under graphene films, Nano Letters 9 (1) (2009) 332–337.

[12] J. S. Bunch, S. S. Verbridge, J. S. Alden, A. M. van der Zande, J. M. Parpia, H. G. Craighead, P. L. McEuen, Impermeable atomic membranes from graphene sheets, Nano Letters 8 (8) (2008) 2458–2462.

[13] S. P. Koenig, N. G. Boddeti, M. L. Dunn, J. S. Bunch, Ultrastrong adhesion of graphene membranes, Nat Nano 6 (2011) 543–546.

[14] J. Zabel, R. R. Nair, A. Ott, T. Georgiou, A. K. Geim, K. S. Novoselov, C. Casiraghi, Raman spectroscopy of graphene and bilayer under biaxial strain: Bubbles and balloons, Nano Letters 12 (2) (2012) 617–621.

[15] E. Khestanova, F. Guinea, L. Fumagalli, A. K. Geim, I. V. Grigorieva, Universal shape and pressure inside bubbles appearing in van der waals heterostructures, Nature Communications 7 (2016) 12587 EP –.

[16] K. Xu, P. Cao, J. R. Heath, Scanning tunneling microscopy characterization of the electrical properties of wrinkles in exfoliated graphene monolayers, Nano Letters 9 (2009) 4446–4451.

[17] N. Levy, S. A. Burke, K. L. Meaker, M. Panlasigui, A. Zettl, F. Guinea, A. H. C. Neto, M. F. Crommie, Strain-induced pseudo-magnetic fields greater than 300 tesla in graphene nanobubbles, Science 329 (5991) (2010) 544–547.

[18] J. L. Garcia-Pomar, A. Y. Nikitin, L. Martin-Moreno, Scattering of graphene plasmons by defects in the graphene sheet, ACS Nano 7 (6) (2013) 4988–4994.

[19] A. Castellanos-Gomez, R. Roldán, E. Cappelluti, M. Buscema, F. Guinea, H. S. J. van der Zant, G. A. Steele, Local strain engineering in atomically thin mos2, Nano Letters.

[20] R. Ruoff, Perspective: A means to an end, Nature 483 (7389) (2012) S42.

[21] V. M. Pereira, A. H. Castro Neto, H. Y. Liang, L. Mahadevan, Geometry, mechanics, and electronics of singular structures and wrinkles in graphene, Phys. Rev. Lett. 105 (2010) 156603.

[22] K. Zhang, M. Arroyo, Understanding and strain-engineering wrinkle networks in supported graphene through simulations, Journal of the Mechanics and Physics of Solids 72 (0) (2014) 61 – 74.

[23] X. Liu, N. G. Boddeti, M. R. Szpunar, L. Wang, M. A. Rodriguez, R. Long, J. Xiao, M. L. Dunn, J. S. Bunch, Observation of pull-in instability in graphene membranes under interfacial forces, Nano Letters 13 (5) (2013) 2309–2313.

[24] W. Pan, J. Xiao, J. Zhu, C. Yu, G. Zhang, Z. Ni, K. Watanabe, T. Taniguchi, Y. Shi, X. Wang, Biaxial compressive strain engineering in graphene/boron nitride heterostructures, Sci. Rep. 2 (2012) 893.

[25] P. Wang, W. Zhang, O. Liang, M. Pantoja, J. Katzer, T. Schroeder, Y.-H. Xie, Giant optical response from graphene–plasmonic system, ACS Nano 6 (7) (2012) 6244–6249.

[26] T. Georgiou, L. Britnell, P. Blake, R. V. Gorbachev, A. Gholinia, A. K. Geim, C. Casiraghi, K. S. Novoselov, Graphene bubbles with controllable curvature, Applied Physics Letters 99 (9) (2011) 093103.

[27] E.-A. Kim, A. H. C. Neto, Graphene as an electronic membrane, EPL (Europhysics Letters) 84 (5) (2008) 57007.

[28] F. Guinea, M. I. Katsnelson, A. K. Geim, Energy gaps and a zero-field quantum hall effect in graphene by strain engineering, Nat Phys 6 (2010) 30–33.

[29] N. G. Boddeti, X. Liu, R. Long, J. Xiao, J. S. Bunch, M. L. Dunn, Graphene blisters with switchable shapes controlled by pressure and adhesion, Nano Letters 13 (12) (2013) 6216–6221.

[30] A. L. Kitt, Z. Qi, S. Rémi, H. S. Park, A. K. Swan, B. B. Goldberg, How graphene slides: Measurement and theory of strain-dependent frictional forces between graphene and sio2, Nano Letters 13 (6) (2013) 2605–2610.

[31] K. Yue, W. Gao, R. Huang, K. M. Liechti, Analytical methods for the mechanics of graphene bubbles, Journal of Applied Physics 112 (8) (2012) –.

[32] M. Arroyo, T. Belytschko, An atomistic-based finite deformation membrane for single layer crystalline films, Journal of the Mechanics and Physics of Solids 50 (9) (2002) 1941–1977.

[33] M. Arroyo, T. Belytschko, Finite element methods for the nonlinear mechanics of crystalline sheets and nanotubes., Int. J. Numer. Meth. Engng 59 (3) (2004) 419–456.

[34] K. Zhang, M. Arroyo, Adhesion and friction control localized folding in supported graphene, Journal of Applied Physics 113 (19) (2013) 193501.

[35] Z. H. Aitken, R. Huang, Effects of mismatch strain and substrate surface corrugation on morphology of supported monolayer graphene, Journal of Applied Physics 107 (12) (2010) 123531.

[36] P. Wang, W. Gao, R. Huang, Entropic effects of thermal rippling on van der waals interactions between monolayer graphene and a rigid substrate, Journal of Applied Physics 119 (7).

[37] L. D. Landau, E. M. Lifshitz, Theory of Elasticity, Pergamon, 1959.